Chemistry & Biodiversity

WILEY-VCH

CHEMISTRY & BIODIVERSITY

RESEARCH ARTICLE

Activity of Sesquiterpene Lactones and Umbelliferone From *Campovassouria cruciata* on SARS-CoV-2 Replication and on the Release of Pro-Inflammatory Cytokines in Lung Cells

Maria Beatriz O. de Rabelo[1] | Kátia M. Freitas[2] | Leonardo C. de Oliveira[3] | Alessandra C. M. Frade[1] | José D. de S. Filho[4] | Gustavo Heiden[5] | Geraldo W. Fernandes[6] | Izabella Thaís Silva[7] | Mauro Martins Teixeira[3] | Fernão C. Braga[1] | Rodrigo M. Pádua[1]

[1]Department of Pharmaceutical Sciences, Faculty of Pharmacy, Universidade Federal de Minas Gerais, Belo Horizonte, Minas Gerais, Brazil | [2]Department of Pharmacology, Institute of Biological Sciences, Universidade Federal de Minas Gerais, Belo Horizonte, Brazil | [3]Department of Biochemistry and Immunology, Institute of Biological Sciences, Universidade Federal de Minas Gerais, Belo Horizonte, Brazil | [4]CiPharma—Programa de Pós-graduação em Ciências Farmacêuticas, School of Pharmacy, Universidade Federal de Ouro Preto, Ouro Preto, Brazil | [5]Herbário ECT—Embrapa Clima Temperado, Pelotas, Rio Grande do Sul, Brazil | [6]Department of Genetics, Ecology and Evolution, Institute of Biological Sciences, Universidade Federal de Minas Gerais, Belo Horizonte, Brazil | [7]Laboratory of Applied Virology, Department of Microbiology, Immunology, and Parasitology, Universidade Federal de Santa Catarina, Florianópolis, Brazil

Correspondence: Rodrigo M. Pádua (rodrigomaiapadua@ufmg.br)

Received: 30 October 2024 | **Revised:** 16 February 2025 | **Accepted:** 21 March 2025

Funding: CAPES (Brazil) is acknowledged for a postdoctoral fellowship (K.M.F.) and the Conselho Nacional de Pesquisa (CNPq/Brazil) for a research fellowship (F.C.B.) (CNPq 312326-2021-1). We acknowledge the Fundação de Amparo à Pesquisa do Estado de Minas Gerais (FAPEMIG/Brazil) for the financial support to the NMR spectroscopy facility (LAREMAR/UFMG; Grant APQ-01848-22) and for a PhD fellowship (M.B.O.R.).

Keywords: anti-inflammatory | antiviral | sesquiterpene lactones | severe acute respiratory syndrome coronavirus 2 (SARS-CoV-2)

ABSTRACT

The investigation of natural products is a valid strategy to identify compounds active against coronaviruses. We herein report the screening of *Baccharis* and *Campovassouria* plant species against the murine betacoronavirus murine hepatitis virus-3 (MHV-3), assays that can be carried out in BSL-2 facilities. These genera occur exclusively in the Americas and are a source of secondary metabolites with antiviral and anti-inflammatory activity. *Campovassouria cruciata* emerged as the most active species from the screening, and its phytochemical investigation afforded the discovery of a new isomer of leptocarpin, 3-*epi*-leptocapin (**1**), in addition to the sesquiterpenes lactones leptocarpin (**2**) and arturin (**3**), along with umbelliferone (**4**). The structures were elucidated by extensive mono- and two-dimensional ^{1}H and ^{13}C NMR data analysis. The antiviral activity of the isolated compounds was also assayed in Calu-3 cells infected with severe acute respiratory syndrome coronavirus 2 (SARS-CoV-2). All compounds inhibited SARS-CoV-2 replication, with a reduction in viral load of approximately 1.7–2.0 log when tested at 7.5 μM. To evaluate potential anti-inflammatory activity, compounds were tested in A549 cells stimulated with IFN-γ and TNF-α. Both 3-*epi*-leptocarpin (**1**) and umbelliferone (**4**) inhibited interleukin-6 (IL-6) and IL-8 release significantly. Compound **1** reduced the production of reactive oxygen species (ROS) in A549 cells, as assessed by flow cytometry using DCFH-DA, whereas **4** exhibited ROS values seven-fold higher than the basal level. Our results highlight *C. cruciata* as a source of promising bioactive compounds, which deserve future investigations to explore their potential for the development of new therapeutic agents against inflammatory and viral diseases.

1 | Introduction

Since the advent of the 21st century, three distinct strains of coronavirus have been identified as etiological agents of lethal pneumonia in humans: severe acute respiratory syndrome coronavirus (SARS-CoV) [1, 2], Middle East respiratory syndrome coronavirus (MERS-CoV) [3, 4], and the more recent one, SARS-CoV-2, responsible for the pathogenesis of coronavirus disease 2019 (COVID-19) [5, 6]. In March 2020, the World Health Organization (WHO) officially classified COVID-19 as a pandemic, which, until June 2024, resulted in more than 700 million cases and more than 7 million deaths worldwide [7].

The rapid proliferation of the disease has prompted an urgent quest for effective therapeutic interventions against SARS-CoV-2. Numerous drugs have been repurposed or employed on the basis of their in vitro efficacy or previous clinical success in managing diseases caused by coronaviruses [8]. For example, remdesivir, ritonavir, lopinavir, ribavirin, and dexamethasone (DX) have been utilized to reduce symptoms in COVID-19 patients. However, these medications carry various adverse effects, including liver damage associated with remdesivir [9]. Although vaccines are the most effective strategy for controlling SARS-CoV-2, there are concerns about their effectiveness against new variants [10].

In this context, natural products represent a valid strategy to identify new antiviral compounds [11]. Some examples of antiviral drugs that used natural products as prototypes are oseltamivir, zanamivir, and laninamivir, used to treat influenza [12]. Natural products from plants, animals, and marine organisms have been extensively investigated and hold significance in COVID-19. Some of these compounds not only reduce viral replication but also regulate inflammatory responses and modulate the immune system [13]. Examples include tylophorine, an alkaloid demonstrating notable inhibitory effects against SARS-CoV-2 in Vero cells along with baicalin and baicalein, which have exhibited virus inhibition in the same model [14].

The Asteraceae family stands out as one of the largest families among flowering plants, with a global distribution that encompasses numerous medicinal species [15, 16]. Within this family, *Baccharis* and *Campouvassouria* are two genera found exclusively in the Americas, particularly prevalent in high-altitude regions [17, 18]. *Baccharis* L. is distributed throughout the Brazilian territory, with several species traditionally employed for medicinal purposes [19]. Among these, *B. dracunculifolia* and *B. trimera* have been well investigated for their medicinal properties. In contrast, the genus *Campovassouria* is limited to South America, found in Bolivia, Paraguay, Argentina, and Uruguay. Within Brazil, its range extends from the Northeast to the South regions [18]. Although the chemistry of *Campovassouria* has not been extensively explored, it shares similarities with *Disynaphia, Grazielia*, and *Eupatorium* genera, all of them belonging to the Eupatorieae tribe [20, 21].

Previous studies on *Baccharis* species have revealed the presence of uncommon polyphenols that are potential inhibitors of SARS-CoV-2. These compounds have demonstrated the ability to hinder the virus from entering the host cell, impede replication, or disrupt protein synthesis, as indicated by in silico studies [22]. Additionally, herbacetin and pectolinarin have inhibited in vitro the main viral protease 3CLpro [23], whereas myricetin has shown significant efficacy as an RdRp antagonist [24]. Retusin, in turn, has inhibited SARS-CoV-2 replication in Vero E6 and Calu-3 cells [25]. The *Campouvassouria* genus has also been recognized as a potential source of antiviral compounds. Unlike *Baccharis* species, the bioactive compounds identified in *Campouvassouria* species are sesquiterpene lactones. Some sesquiterpene lactones structurally alike to the germacralides, guaianolides, and heliangolides identified in the genus [26] have been investigated for their biological activities. For instance, reynosin, artemisinin, and tagitinins have been found to inhibit SARS-CoV-2 proteins, as well as pro-inflammatory mediators [27–30].

In order to explore que antiviral potential of *Baccharis* and *Campouvassouria*, we herein report a screening of plant extracts from these genera against the murine coronavirus murine hepatitis virus-3 (MHV-3). *Campovassouria cruciata* emerged as the most active species and its phytochemical study afforded a new isomer of leptocarpin, **3-epi-leptocapin** (1), in addition to the sesquiterpene lactones **leptocarpin** (2) and **arturin** (3), along with **umbelliferone** (4). The chemical structures of the isolated compounds were established unambiguously through comprehensive analysis of their NMR data and comparison with literature records. The effects of the extract and isolated compounds on the release of pro-inflammatory cytokines were evaluated in vitro, alongside their antiviral activity against SARS-CoV-2.

2 | Results and Discussion

2.1 | Antiviral Screening Against Coronavirus MHV-3

The antiviral effects of extracts from *Baccharis brevifolia*, *Baccharis calvescens*, *Baccharis imbricata*, *Baccharis oblongifolia*, *Baccharis stylosa*, and *C. cruciata* were evaluated in L929 cells infected with MHV-3. Initially, the viability of L929 cells was examined following treatment with these extracts at concentrations ranging from 10 to 90 μg/mL using the MTT (3-(4,5-dimethylthiazol-2-yl)-2,5-diphenyltetrazolium bromide) assay. Similarly, the cytotoxicity of fractions derived from *C. cruciata* extract was assessed in L929 cells within the same concentration range. Concentrations demonstrating 90% cell viability were considered non-cytotoxic (Figure S1) and were subsequently utilized in the antiviral assays.

The antiviral screening was carried out on L929 cells infected with the MHV-3. This coronavirus is recognized as a valid model for testing potential SARS-CoV-2 inhibitors, in view of their structural and genomic similarities, along with the disease manifestation in murine that resembles the COVID-19 pathogenesis in humans [31]. The rationale for using the MHV-3 model in antiviral screening lies in its practicality and safety advantages for early-stage experiments. Unlike SARS-CoV-2, which requires high-level biosafety containment (BSL-3 or higher), MHV-3 can be handled in lower biosafety levels, making it more accessible and cost-effective for preliminary assessments. The inhibitory activity of the extracts at 10 and 30 μg/mL against MHV-3 replication was evaluated in L929 cells infected with MHV-3 at the multiplicity of infection (MOI) of 0.01. Viral yields in both treated and untreated monolayers were determined by plaque assay. The

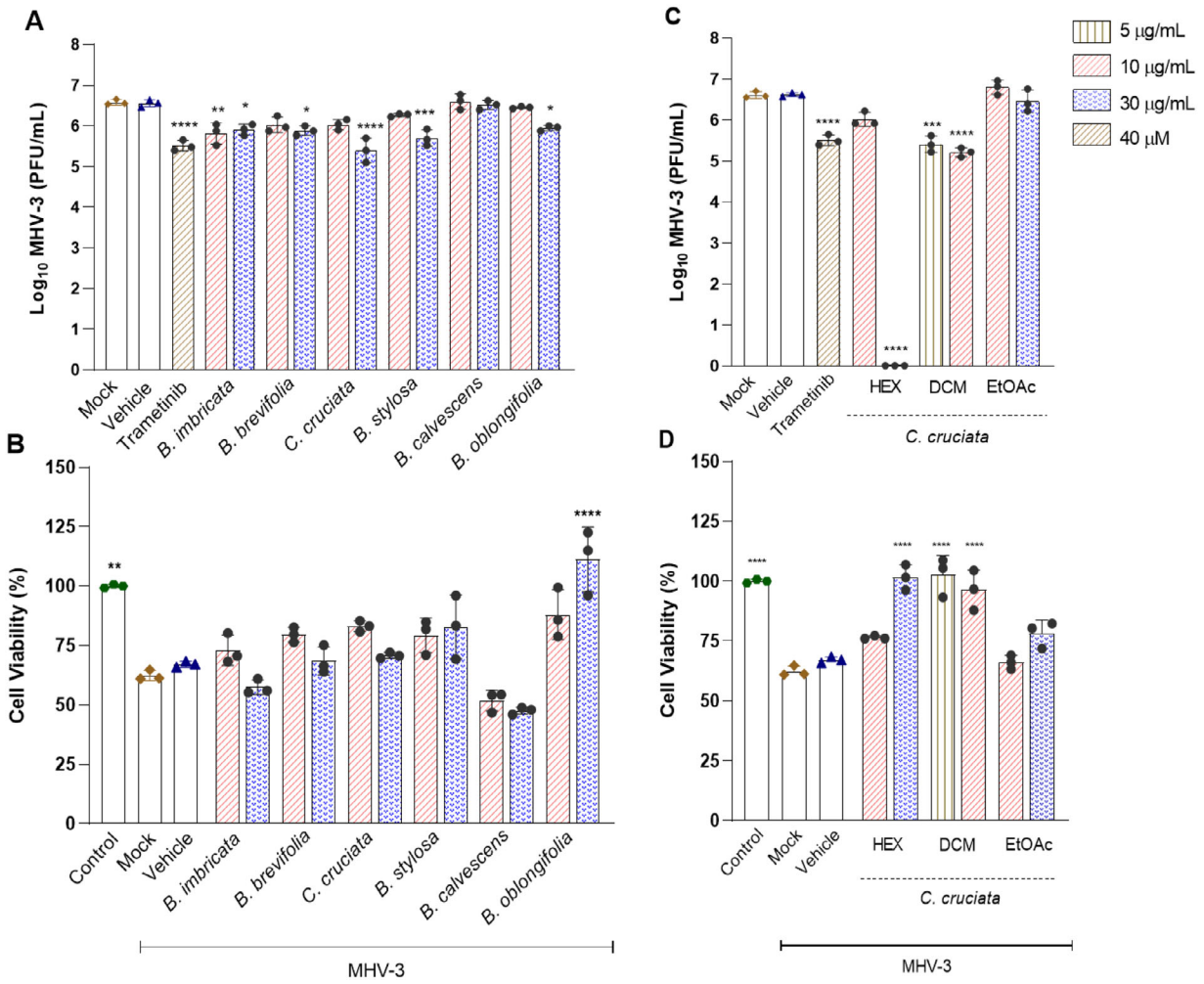

FIGURE 1 | Effect of the extracts and *Campovassouria cruciata* fractions on the viral loads of MHV-3-infected L929 fibroblasts. Plaque assays were performed with supernatants from L929 cells (10^5 cells/well) infected with MHV-3 (MOI 0.01) for 16 h and titrated on L929 cells overlaid with 0.8% carboxymethylcellulose. Cells were pre- and post-treated after infection. (A) Effect of extracts at 10 and 30 µg/mL, on MHV-3 infection; (B) cell viability after 16 h post-treatment with extracts; (C) effect of *C. cruciata* fractions at 10 and 30 µg/mL on MHV-3 infection; (D) cell viability after 16 h post-treatment with fractions. The data obtained were expressed in plaque-forming units per milliliter (PFU/mL) and % cell viability, compared with group Vehicle (DMSO + ethanol) (mock: cell + virus) (positive control: trametinib—40 µM) ($n = 3$) (*$p < 0.5$; **$p < 0.01$; ***$p < 0.001$; and ****$p < 0.0001$—ANOVA with Tukey post-test). DCM, dichloromethane; EtOAc, ethyl acetate; HEX, *n*-hexane.

cytotoxicity after treatment with the extracts was evaluated by the MTT viability assay.

All tested extracts, with the exception of *B. calvescens*, elicited a decrease in viral titer, notably *C. cruciata* at 30 µg/mL, which resulted in a one log-reduction compared to the vehicle (Figure 1A). Additionally, cell viability ($p > 0.05$) after treatment with this extract was comparable to the infected control, suggesting that the extract was non-toxic to the infected cells (Figure 1B). The extract of *C. cruciata* was fractionated by partition between immiscible solvents, and the resulting fractions were evaluated for their antiviral activity against MHV-3 (Figure 1C). The dichloromethane (DCM) fraction was tested at lower concentrations (5 and 10 µg/mL) due to its observed cell viability below 90% at 30 µg/mL. Both the *n*-hexane (HEX) and DCM fractions exhibited a significant antiviral effect and restored cell viability similarly to the control, whereas the ethyl acetate (EtOAc) fraction did not reduce viral titer at the assayed concentrations (Figure 1D).

2.2 | Effect of *C. cruciata* Extract and Fractions on the Release of Cytokines in A549 Cells

Subsequently, we explored the potential anti-inflammatory activity of the extract and fractions from *C. cruciata*. Acute respiratory distress syndrome (ARDS) caused by coronaviruses like SARS-CoV-2 arises from dysregulated cytokine production—named "cytokine storm"—contributing to the exacerbation of clinical symptoms and ultimately leading to death. Hence, there is significant interest in identifying novel antiviral agents capable of simultaneously controlling the release of pro-inflammatory cytokines.

In cell cultures, respiratory epithelial cells (A549, bronchial epithelium transformed with Ad12-SV40 2B cells [BEAS-2B], and Calu-3) or primary cells exhibit similar expression patterns of molecules associated with SARS-CoV-2 entry, as highlighted by single-cell RNA sequencing (scRNA-seq) or immunostaining [32]. Often, studies on respiratory viruses such as respiratory

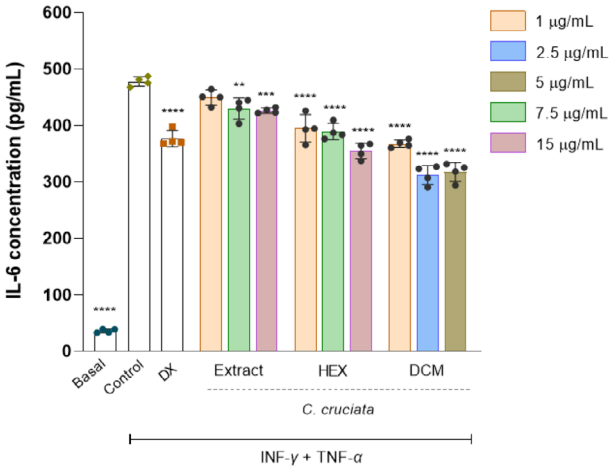

FIGURE 2 | Levels of the pro-inflammatory cytokine IL-6 released by A549 cells previously stimulated by IFN-γ and TNF-α and treated subsequently with the extract and fractions of *Campovassouria cruciata*. The cytokines were measured according to the R&D system immunoassay kit protocol. The results are presented as the mean ± standard deviation of values (pg/mL), compared to the control group (cells stimulated with IFN-γ and TNF-α) (positive control: DX—dexamethasone 10 µM) ($n = 4$) (**$p < 0.01$; ***$p < 0.001$; and ****$p < 0.0001$—ANOVA with Tukey's post-test). DCM, dichloromethane; HEX, *n*-hexane.

syncytial virus and influenza virus utilize the A549 epithelial cell line [33]. Therefore, we stablished an in vitro pulmonary inflammation model on A549 cells to investigate potential antiviral candidates capable of mitigating the manifestations and symptoms of COVID-19.

Our in vitro model involved stimulating A549 cells simultaneously with IFN-γ and TNF-α. These pro-inflammatory mediators were chosen due to their significant role in the progression and exacerbation of COVID-19. IFN-γ was previously identified as a mediator of inflammation and coagulation in SARS [34], and elevated levels of interleukin-6 (IL-6) serve as a pertinent parameter for predicting the unfavorable course of COVID-19 [35]. The mitigation of cytokine release induced by the test samples was assessed by quantifying the levels of IL-6 and TNF-α released by the cells. Following stimulation with IFN-γ and TNF-α, A549 cells exhibited a 3.75-fold increase in IL-6 levels (300.3 ± 5.326 vs. 81.43 ± 0.901 picograms per milliliter (pg/mL) in the basal group, $p < 0.0001$) and a 33-fold increase in TNF-α levels (535.3 ± 15.86 vs. 16.14 ± 1.027 pg/mL in the basal group, $p < 0.0001$) throughout the assay period (24 h) (data not shown).

Initially, A549 cells were treated with extracts and fractions of *C. cruciata*, and the cell viability was assessed by MTT assay (Figure S2). The extract and the HEX fraction demonstrated >90% cellular viability at concentrations up to 15 µg/mL, whereas for the DCM fraction, this threshold was observed at 5 µg/mL. The HEX and DCM fractions were selected for assay because they exhibited promising activity against MHV-3.

The extract and its derived fractions reduced IL-6 secretion by A549 cells (Figure 2), with the DCM fraction notably effective. This fraction induced diminished levels of IL-6 at all tested concentrations, resulting in a 20% reduction at 1 µg/mL compared to the control group (cells + cytokines). Additionally, the DCM fraction at 2.5 and 5 µg/mL reduced IL-6 secretion approximately 15% more than DX, an anti-inflammatory used as positive control. The basal condition was utilized to establish a control state without any external stimuli or interventions.

It is well established that several phytoconstituents possess immunomodulatory properties, facilitating the upregulation of anti-inflammatory cytokine expression while concurrently down-regulating the expression of inflammatory cytokines, including IL-6, IL-17, and TNF-α [36]. Several plant extracts and compounds isolated thereof have been reported to exhibit anti-inflammatory properties, including species of the Eupatorieae tribe, which encompasses the *Campovassouria* genus. For instance, *Eupatorium perfoliatum* inhibited NO release in RAW 264.7 cells stimulated by lipopolysaccharide (LPS), and the activity was ascribed to eupafolin, a sesquiterpene lactone [37]. Similarly, a fraction of sesquiterpenes derived from *Eupatorium lindleyanum* has been shown to down-regulate the levels of TNF-α, IL-6, and IL-1β in a murine model of LPS-induced acute lung injury [38].

2.3 | Isolation and Structure Elucidation of Constituents From the DCM Fraction

The DCM fraction was selected for further fractionation aiming to isolate its antiviral constituents, demonstrated against MHV-3, and also for its potential anti-inflammatory activity by reducing IL-6 release from A549 cells stimulated by IFN-γ and TNF-α.

The UPLC-DAD profile recorded for the DCM fraction revealed the presence of four major peaks at retention times of 2.65, 4.24, 4.33, and 5.47 min (Figure 3). The other peaks in the analysis were not described in detail because they were identified as flavonoids that are already well known in the scientific literature. Peak 1 exhibited an intense absorption UV band at 323 nm in spectra, suggestive of a coumarin, whereas Peaks 2–4 did not present conjugated chromophores (λ_{max} 215–220 nm). Considering the previous reports of sesquiterpene lactones in this species [26], analysis of the mass spectra of compounds eluted as Peaks 2–4 suggested that they belong to this class. The protonate ion at m/z 363 $[M + H]^+$ observed for Peaks 2 and 3, along with the ion at m/z 263 $[M—C_5H_8O_2 + H]^+$, suggests the loss of a tiglic or angelic group, characteristic of germacrolides, heliangolides, and guainolides previously identified in *C. cruciata*. Similarly, the ions at m/z 347 $[M + H]^+$ and m/z 247 $[M—C_5H_8O_2 + H]^+$ observed for Peak 4 allowed a similar conclusion. The loss of hydroxyl groups was also observed for these compounds (see the Supporting Information section).

Hence, a portion of the DCM fraction was fractionated over a silica gel column to afford a new stereoisomer of leptocarpin (compound **1**) along with the known sesquiterpene lactones **leptocarpin (2)** and **arturin (3)**, in addition to **umbelliferone (4)** (Figure 4).

UPLC-ESI-MS analysis of compound **1** furnished the protonated and deprotonated molecules, respectively, at m/z 363 $[M + H]^+$ and 361 $[M–H]^-$, compatible with the molecular formula $C_{20}H_{26}O_6$. The ^{13}C NMR spectrum of **1** presented resonance signals of 20 carbon atoms, comprising 2 carbonyl groups (169.2

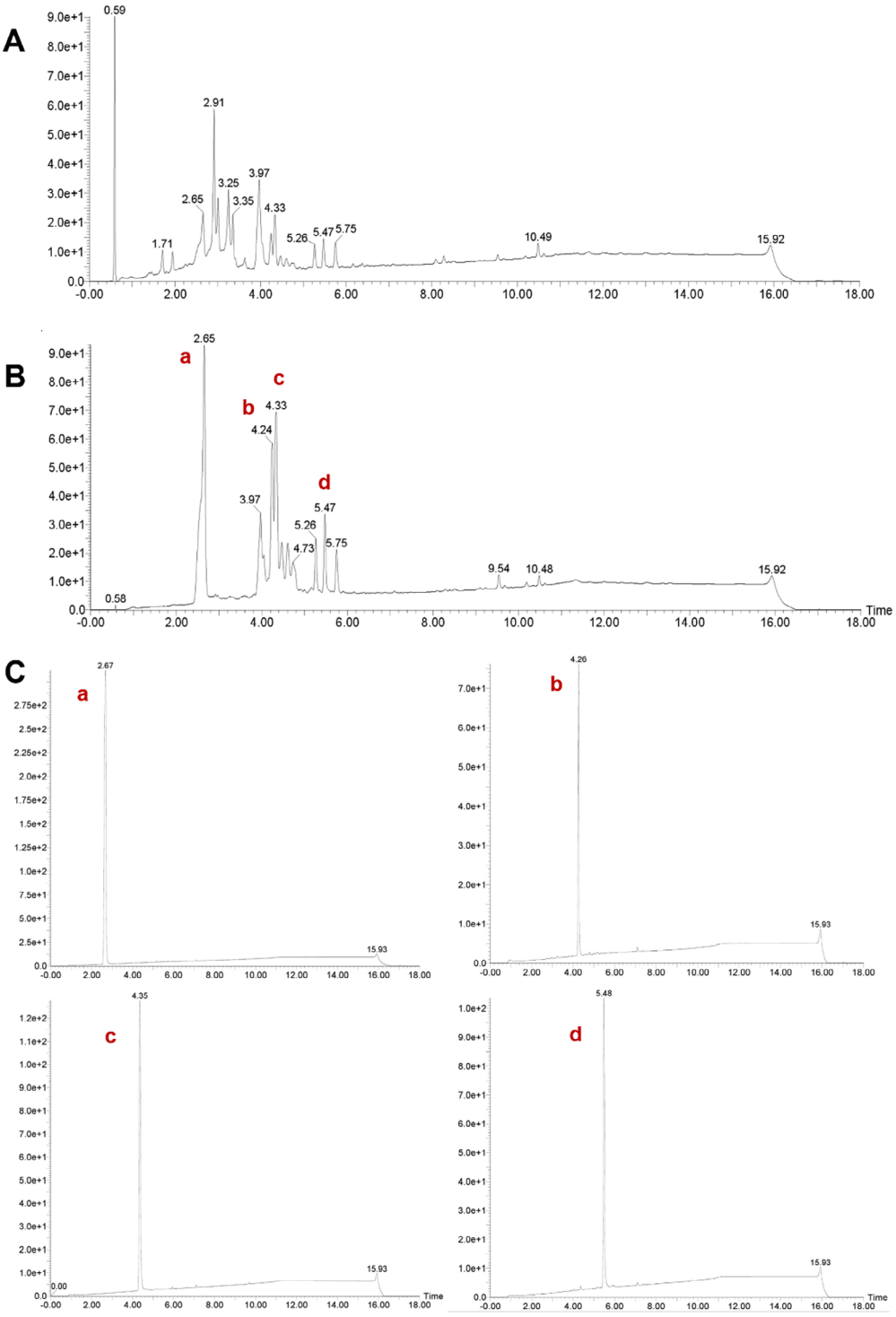

FIGURE 3 | Chromatographic profiles obtained by UPLC-DAD for the ethanolic extract (A), dichloromethane (DCM) fraction (B), and isolated compounds (C) of *Campovassouria cruciata*. (a: umbelliferone; b: 3-epi-leptocapin; c: leptocarpin; d: arturin). Experimental conditions: see Section 4.

and 166.3 ppm), 4 quaternary carbons (141.9, 137.0, 126.6, and 57.1 ppm), 4 methyl, 3 methylene, and 7 methine groups (Table 1), according to DEPT-135 and HSQC data.

The ^{1}H NMR spectrum of **1** revealed two resonance signals at δ_H 5.80 and 6.40 ppm (J = 1.4 Hz), ascribed to the methylene hydrogens of the terminal double bond at C13. The correlation between the carbonyl resonance at 169.2 ppm and the CH_2 signal at 125.3 ppm, disclosed by the HMBC contour map, indicates the presence of an α-methylene-γ-lactone group, commonly found in sesquiterpenes from *Eupatorium* tribe and Disynaphiinae subtribe [21]. Furthermore, the HMBC correlations from the carbonyl (C-12) to the protons at 5.56 (H-6) and 2.91 (H-7) ppm indicate that these two methine groups are, respectively, located at the γ and β positions relative to the carbonyl group.

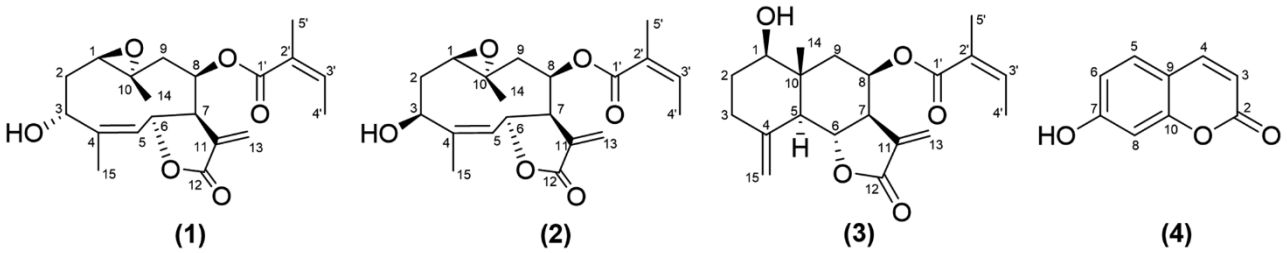

FIGURE 4 | Structures of compounds **1–4**.

The ^{1}H–^{1}H COSY correlation between the doublets at 5.30 ppm (H-5) and 5.56 ppm (H-6) indicates an allylic double bond in the lactone ring. Analysis of the HMBC data revealed a correlation between the carbons at 124.3 ppm (C-4) and 141.9 ppm (C-5) with the proton resonance at 1.87 ppm (H-15), thus confirming the presence of a methyl group attached to C-4. Additionally, the magnitude of the coupling constant $J_{5,6}$ (11.0 Hz) and the NOESY correlation between H-5/H-15 allowed the assignment of a *Z*-geometry to the C-4/C-5 double bond.

From the observation of two vinylic methyl groups at 1.98 (H-4′) and 1.87 ppm (H-5′), together with an olefinic proton at 6.14 ppm (H-3′), it was possible to infer the presence of the angeloyl group. The coupling constant $J_{3',4'}$ 7.2 Hz supports the presence of a geminal proton to a methyl group, and the olefinic proton signal around 6.10 ppm is characteristic of angelates [39]. Moreover, the NOESY correlation between H-3′ and H-5′ corroborates the presence of an angeloyl group. The HMBC correlations from C-2′ (126.6 ppm) and C-3′ (141.0 ppm) to the resonances of H-4′ (1.98 ppm, d $J = 7.2$ Hz) and H-5′ (1.87 ppm, s) confirm the two methyl groups as substituents of the double bond. Furthermore, the HMBC correlation from the carbonyl signal at 166.3 ppm (C-1′) with H-3′ and H-8 supports the presence of the angeloyl ester and its attachment to C-8. The resonance signals at 58.6 and 57.1 ppm, respectively, assigned to C-1 and C-10, indicate the presence of an oxirane group between these atoms. In turn, carbinol resonance at 66.5 ppm was ascribed to C-3, pointing out the location of a hydroxyl at this position.

Sesquiterpene lactones are formed through the condensation of three isoprene units, followed by cyclization and oxidative transformation, resulting in a *cis*- or *trans*-fused lactone [40]. All heliangolides, germacrolides, and guaianolides previously isolated from *C. cruciata* exhibit a *trans*-fused lactone ring, where H-7 is consistently α-oriented without exception [41]. In compound **1**, the correlation observed between H-7/H-1 and H-7/H-8 in the NOESY spectrum enabled the determination of the α-orientation of both H-1 and H-8. Although there are NOESY correlations between H-6 and H-7, it is important to highlight that the H-7 signal appears as a broad singlet from a small coupling constant, indicating an *anti*-arrangement, with H-6 in β-orientation. Therefore, the correlation between H-6/H-14 and H-6/H-3, evidenced in NOESY spectrum, suggests the β-orientation of both the 14-methyl group and H-3 (see the Supporting Information section).

The relative stereochemistry of compound **1** was established by NOESY correlations (Figure 5) between H-7/H-1 and H-6/H-14, demonstrating the *trans*-fusion of the oxirane ring, and between H-7/H-8, indicating the β-orientation for the angeloyloxy group. The strong correlation between H-6/H-3 and H-14/H-3 assigned the α-orientation of the hydroxyl group at C-3. Therefore, the structure of **(1)** was assigned as 8β-angeloyloxy-3α-hydroxy-1α,10-epoxy-6βH,7αH-helianga-4Z,11(13)-dien-6,12-olide, or **3-epi-leptocarpin**, which is described here for the first time.

Compound **2** produced the protonated and deprotonated ions, respectively, at *m/z* 363 $[M + H]^+$ and 361 $[M–H]^-$ according to UPLC-ESI-MS analysis, consistent with the molecular formula of $C_{20}H_{26}O_6$. The spectroscopic data obtained for **2** show similarities with compound **1** in relation to α,β-unsaturated lactone, *Z*-configuration of C-4/C-5 double bond, 1,10-oxirane ring, and the 8β-angeloyloxy group. The differences detected in the NMR data were in the C-3 and C-15 signals, which resonate at 66.5 and 17.1 ppm in **1,** whereas they resonate at 72.3 and 23.1 ppm in **2** (Table 1). Moreover, H-3 showed a slight shift and a change of the multiplicity from a double doublet to a broad singlet. The H-6 proton signal resonates at 5.56 ppm in compound **1** and at 6.66 ppm in **2**. This shift difference in the H-6 proton signal is also observed in isomers that have α- or β-positioned hydroxyl group. For example, heliangin, the hydroxyl group of which at C-3 is β-positioned, has the H-6 shift at 6.67 ppm, whereas in 3-*epi*-heliangin, with OH-3 α-positioned, has H-6 shift at 5.59 ppm [42]. According to Holub and Samek [43] this change in the chemical shift, which also occurs in nobilin (β OH-3) and 3-*epi*-nobilin (α OH-3), indicates the van der Waals repulsion effect of the hydroxyl electrons at C-3 on the proton H-6, which is only possible considering the *Z* configuration of the double bond between C-4 and C-5. The NOESY data confirm the β-orientation for the angeloyloxy and 14-methyl groups by the correlations between H-7/H-8 and H-6/H-14, respectively. In addition, the cross-peak between H-6/OH-3 supports the β-orientation of the hydroxy group at C-3 (Figure 5).

Taken together, the obtained spectroscopic data indicate that compound **2** is **leptocarpin**, a compound previously isolated from *Leptocarpha rivularis* exhibiting the characteristic stereochemistry of heliangolides. The molecular structure of **leptocarpin** and **leptocarpin acetate** was established by single-crystal x-ray diffraction, and its absolute configuration was derived from cryptographic data [39, 44, 45]. To confirm the stereochemistry of compounds **1** and **2**, electronic circular dichroism (ECD) spectra were recorded. The CD spectrum of **1** and **2** exhibited a positive band at 240 nm, indicative of a positive Cotton effect of the $n \rightarrow \pi^*$ transition of the α-methylene-γ-lactone group, as previously demonstrated by Ober et al. [44] for leptocarpin acetate. On the other hand, **1** and **2** presented opposite band signals around 200 nm, namely, negative for **2** and positive for

TABLE 1 | ^{1}H NMR and ^{13}C NMR ($CDCl_3$, 600 MHz, *J* in Hz) spectroscopic data of compounds **1–3** and comparison with leptocarpin and arturin data [44–46].

Position	1[a]		2[a]		3[a]		Leptocarpin[a]		Arturin[a]
1	2.8, m	59.6	2.83, m	60.8	3.53, dd (4.6, 11.3)	78.6	2.80, dd (5.9)	60.68	3.54, dd (4.5, 11.0)
2	1.68, m 2.36, td (5.0, 13.0)	34.4	1.73, m (2.4, 10.3, 15.0) 2.44, dt (4.3, 14.8)	32.6	1.59, m 1.82, m	30.9	1.75, m (2.0, 9.0, 15.0) 2.45, dt (5.5, 15.0)	32.53	1.64, m (6.0, 13.0) 1.93, m (1.5, 6.0)
3	4.95, dd (5.0, 11.0)	66.5	4.49, s	72.3	2.14, td (5.0, 12.5) 2.35, m (5.0, 14.0)	33.4	4.50, dd (2.0, 5.0)	72.22	2.15, td (6.0, 13.0) 2.37, td (1.5; 3.0, 13.0)
4		141.9		141.5		141.9		141.65	
5	5.30, d (10.5)	124.3	5.32, d (10.8)	126.5	2.27, d (11.0)	53.5	5.31, dd (2.0, 11.0)	126.39	2.28, d (11.0)
6	5.56, dd (2.5, 11.0)	73.0	6.66, dd (2.0, 10.8)	74.3	4.51, t (11.0)	75.3	6.70, dd (2.0, 11.0)	74.17	4.52, dd (11.0)
7	2.91, s	48.8	2.9, s	48.5	2.86, dq (11.0)	52.1	3.00, m	48.44	2.87, m (2.5, 3.0, 11.0)
8	5.23, s	75.5	5.20, s	75.9	5.82, m (3.0)	65.6	5.25, m	75.82	5.84, td (2.5)
9	1.30, dd (2.0, 13.5) 2.81, dd (4.2, 15.0)	43.1	1.34, dd (2.0, 15.0) 2.82, m	437	1.63, m 2.40, dd (2.0, 15.0)	40.4		43.63	1.64, m (2.5; 15.0) 2.41, td (2.1, 5.1, 13.7)
10		57.1		58.8		42.8		58.70	
11		137.0		137.5		134.6		126.93	
12		169.2		169.7		169.9		169.58	
13	5.80, d (1.5) 6.40, d (1.5)	125.3	5.78, d (2.0) 6.36, d (2.0)	124.9	5.49, d (3.0) 6.17, d (3.0)	119.7	5.70, d (2.0) 6.30, d (2.0)	124.74	5.50, d (3.0) 6.18, d (3.2)
14	1.51, s	18.6	1.48, s	19.8	0.97, s	13.5	1.50, s	22.94	0.98, s
15	1.87, s	17.1	1.80, s	23.1	4.95, s 5.02, s	110.9	1.80, s	20.33	4.96, d (0.9) 5.04, d (0.9)
1’		166.3		166.5	—	166.9		166.42	
2’		126.9		126.9	—	127.2		137.42	
3’	6.14, q (7.2)	140.5	6.11, q (7.2)	140.5	6.10, dq (1.5, 7.2)	139.6	6.08, m	—	6.11, m (1.5; 7.0)
4’	1.98, d (7.2)	15.9	1.98, dd (1.0, 7.2)	15.8	1.98, dd (1.4, 7.2)	16.0	2.00, m	19.67	1.93, dd (1.5; 7.0)
5’	1.87, s	20.5	1.86, s	20.5	1.85, s	20.7	1.93, m	15.70	1.86, s

[a]Data measured in $CDCl_3$; *J* values are in parentheses and reported in Hz; chemical shifts are given in ppm; assignments were confirmed by COSY, HSQC, and HMBC experiments.

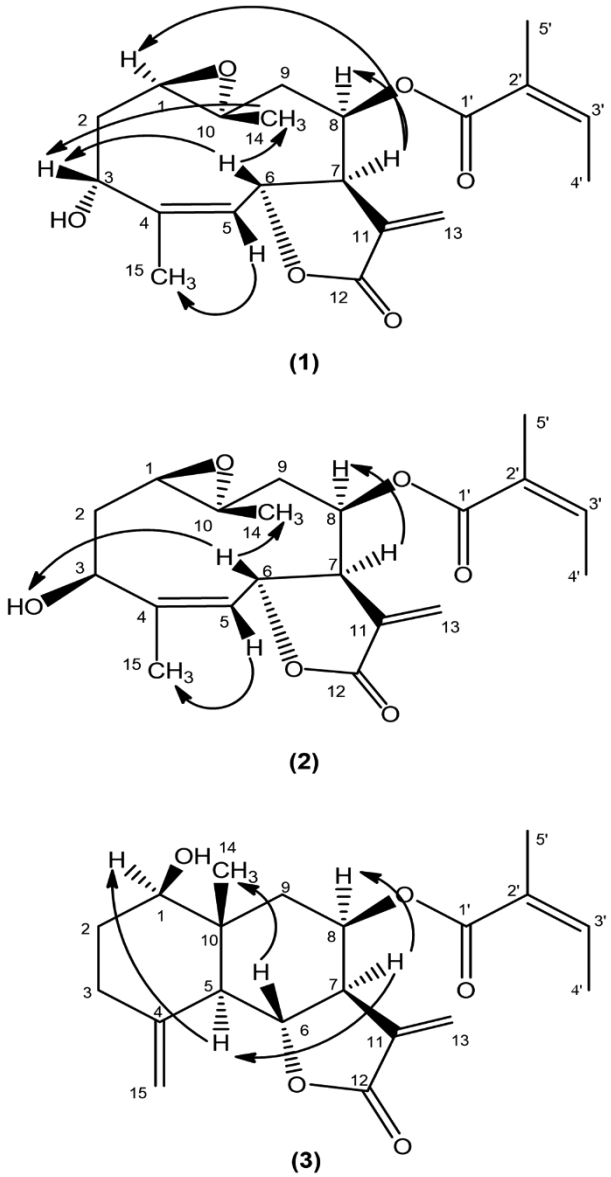

FIGURE 5 | NOESY correlations observed in compounds **1–3**.

1, thus indicating that epimerization occurred at carbon 3 (see Supporting Information section).

The NMR data obtained for **2** in this study enabled us to reevaluate certain signals that were previously assigned by Ober et al. Specifically, C-11 and C-2′ were initially attributed to the resonance signals at 126.9 and 137.4 ppm, respectively. However, our data suggest a reversal of these chemical shifts, with C-11 resonating at 137.5 ppm and C-2′ at 126.9 ppm. These assignments were corroborated by HMBC correlations observed between C-11 and H-13a/H-13b, as well as between C-2′ and H-4′/H-5′ (see Table S2). Similar confirmation was observed for carbons 14 and 15, previously reported at chemical shifts of 22.9 and 20.3 ppm [44], respectively, whereas our study revealed C-14 at 19.8 ppm and C-15 at 23.1 ppm. These attributions were further supported by HMBC correlations, notably between H-14 and C-1/C-9/C-10 and between H-15 and C-3/C-4/C-5 (see Table S2).

The protonated ions at m/z 347 $[M + H]^+$ and 693 $[2M + H]^+$, as detected by UPLC-ESI-MS analysis of compound **3**, were consistent with arturin, a compound previously described in *Podanthus mitiqui* [46, 47]. Twenty carbon resonance signals were observed in the ^{13}C NMR spectrum of **3**, which were assigned using DEPT-135. The pair of doublets at 5.49 and 6.17 ppm, attributed to H-13a and H-13b, respectively, displayed HMBC correlation with the carbonyl signal at 169.9 ppm, assigned to C-12, thereby confirming the presence of the α-methylene-γ-lactone group. Another exomethylene group was identified by two singlets at 5.03 and 4.95 ppm, with HMBC correlation to 141.9 (C-4), 53.5 (C-5), and 33.4 ppm (C-3), indicating attachment to C-4. Additionally, the two vinylic methyl groups at 1.98 (H-4′) and 1.85 ppm (H-5′), the olefinic proton at 6.10 ppm (H-3′), and signals at 166.9 (C-1′), 127.2 (C-2′), 139.6 (C-3′), 16.0 (C-4′), and 20.7 ppm (C-5′) suggest the presence of an angeloyloxy group. The long-range correlation between C-1′ and H-8 supports the ester attachment to C-8. The HMBC correlation observed between the methyl group at 0.97 ppm (H-14) and resonances at 42.8 (C-10), 40.4 (C-9), 53.5 (C-5), and 78.6 ppm (C-1), along with the correlation of the proton at 2.27 ppm (H-5) with C-10 and C-14, confirms the presence of an eudesmanolide skeleton. The proposed relative stereochemistry of compound **3** was elucidated through a NOESY experiment, where correlations between H-7/H-8 and H-7/H-5 suggested the β-orientation for the angeloyloxy group and the α-orientation of H-5 (Figure 5). Additionally, the correlation between H-6/H-14 and H-1/H-5 indicates the β-orientation of the 14-methyl group and the hydroxyl group at C-1. All signals in the ^1H NMR spectrum were assigned and are consistent with those reported previously [46].

Compound **4** was analyzed using UPLC-ESI-MS, revealing one protonated ion at m/z 163 $[M + H]^+$ and one deprotonated ion at m/z 161 $[M–H]^-$. Additionally, its thin-layer chromatography (TLC) profile displayed a blue fluorescent spot under 365 nm detection wavelength, characteristic of single coumarins [48]. Comparison of ^1H NMR and ^{13}C NMR data with literature references confirms the identity of compound **4** as umbelliferone (7-hydroxycoumarin). Umbelliferone is commonly found in various species of the Apiaceae (Umbelliferae), Asteraceae, and Rutaceae families [49], but it is the first description of its occurrence in *C. cruciata*.

The presence of oxygenated sesquiterpenes, including caryophyllene oxide, globulol, epiglobulol, and germacrene D, and monoterpenes, such as α-pinene, β-pinene, sabinene, and limonene [26, 50], have been demonstrated in the volatile oil of the inflorescences and leaves of *C. cruciata*. Furthermore, some sesquiterpene lactones with germacrolide, heliangolide, and guaianolide carbocyclic skeletons were isolated from the aerial part of this species [26].

2.4 | Activity of Isolated Compounds on the Release of Pro-Inflammatory Cytokines and Reactive Oxygen Species (ROS) Production in A549 Cells

Aiming to investigate the potential anti-inflammatory effect of compounds isolated from the bioactive fraction of *C. cruciata*, they were subjected to in vitro testing in A549 cells. Initially, the viability of A549 cells was assessed after treatment with compounds **1–4** at concentrations ranging from 1 to 15 μM

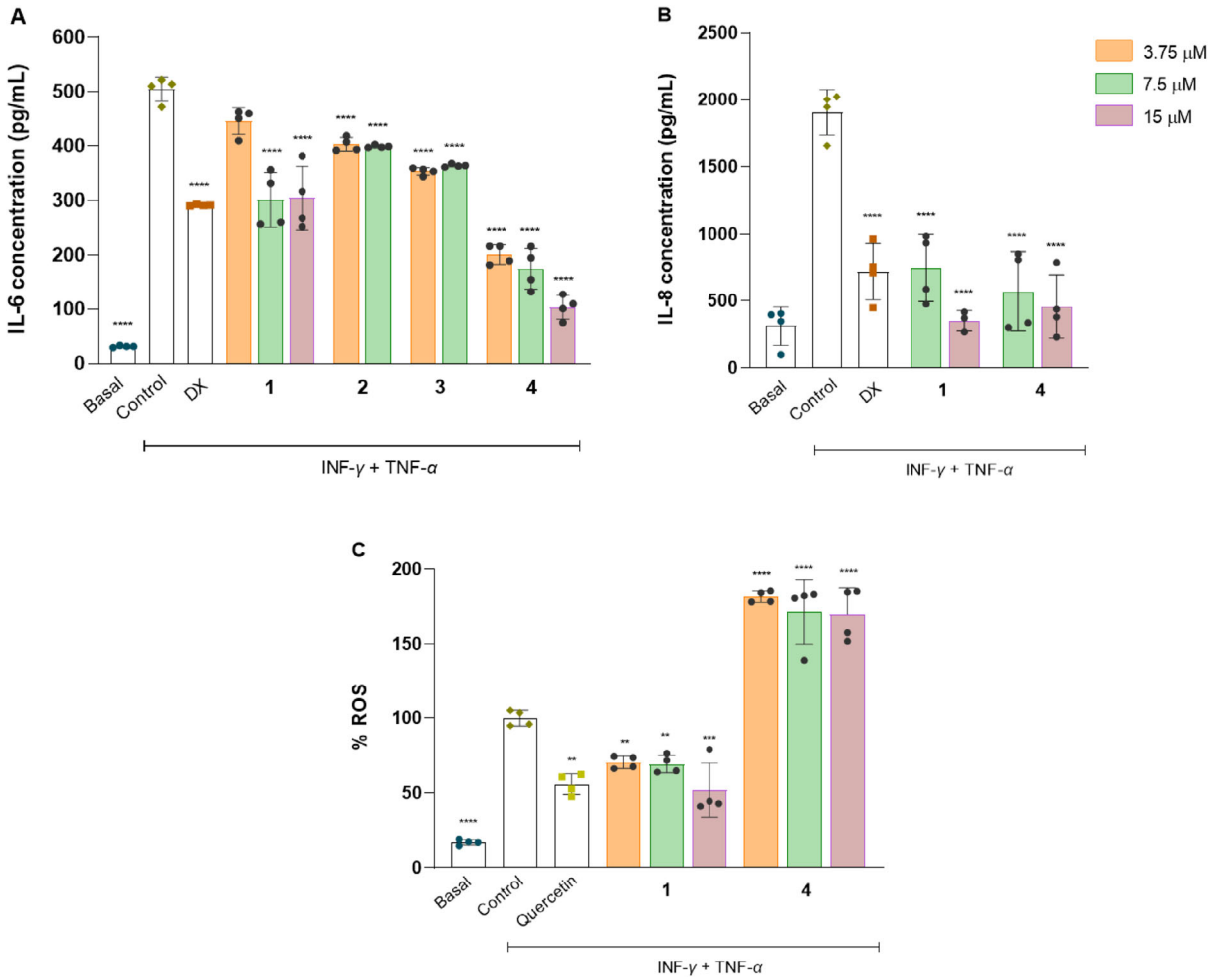

FIGURE 6 | Effect of compounds **1–4** on the release of pro-inflammatory cytokines and intracellular production of ROS in A549 cells previously stimulated with IFN-γ and TNF-α: levels of IL-6 (A) and IL-8 (B) and percentage of ROS (C). The results are presented as the mean ± standard deviation of values, compared with the control group (cells stimulated with IFN-γ and TNF-α); (positive control: DX—dexamethasone 10 μM); (positive control: quercetin 50 μM) ($n = 4$) (**$p < 0.01$; ***$p < 0.001$; and ****$p < 0.0001$—ANOVA with Tukey's post-test).

(Figure S3). Concentrations that resulted in A549 cell viability below 90% were excluded from further evaluation in the assay. All tested compounds demonstrated a significant reduction in IL-6 release by A549 cells previously stimulated with TNF-α and IFN-γ, across the range of concentrations tested. Remarkably, compound **4** exhibited a concentration-dependent inhibition, achieving 79.0% ± 0.2% inhibition at 15 μM compared to the control group, whereas compound **1** demonstrated maximal inhibition of 40.0% ± 0.6% (Figure 6A).

In the subsequent analysis, we assessed the impact of compounds **1** and **4** on the release of IL-8 (Figure 6B) using the same model. Both compounds demonstrated a notable reduction in IL-8 release, with levels dropping by approximately 80% at 15 μM. As IL-8 was identified in patients with mild syndromes, it is also considered a possible marker for the prognosis of the disease [51]. It is noteworthy that compounds **1** and **4** reduced the release of IL-6 and IL-8 to levels comparable to, or higher than, those achieved by the anti-inflammatory agent DX.

Umbelliferone (compound **4**) has been reported to possess antioxidant and anti-inflammatory properties in various models, including animal studies [52]. Compound **4** has shown protective effects against acute lung injury induced by LPS in mice, characterized by reduced infiltration of inflammatory cells and decreased levels of pro-inflammatory cytokines, such as MCP-1, IL-6, IL-1β, and TNF-α [53]. It also attenuated the secretion of pro-inflammatory cytokines and chemokines in HaCat cells exposed to TNF-α/IFN-γ [54]. However, as far as we know, there is no previous report on the effect of umbelliferone in A549 cells under these stimulatory conditions. Although the effects of **leptocarpin** and **arturin** on inflammatory cytokines have never been previously reported, the anti-inflammatory potential and immunoregulatory effects of sesquiterpene lactones have been documented [55]. For instance, tagitinins C, F, and A, isolated from *Tithonia diversifolia*, were found to reduce the production of IL-6, IL-8, and TNF-α induced by LPS in human neutrophil cultures [29]. In evaluations of the anti-inflammatory effects on LPS-activated RAW264 macrophages, eupalinolides L and M, isolated from *E. lindleyanum*, demonstrated reductions in TNF-α and IL-6 levels [30], whereas a eudesmanolide from *Sonchus brachyotus* suppressed the production of TNF-α, IL-6, and IL-10 [56]. Interestingly, compounds **1** and **4** promoted a significant decrease in the release of IL-6 and IL-8 in A549 cells treated with 7.5 and 15 μM, which are markedly lower concentrations than those employed in previous studies with umbelliferone and sesquiterpene lactones.

Viral proteases have been shown to possess the ability to trigger the production of ROS through the TNF-α and NF-$\kappa\beta$ signaling pathways. This complex interaction within the oxidative environment plays various roles depending on the levels of superoxide and its derivatives. This imbalance has the potential to lead to pulmonary injuries, similar to those seen in cases of influenza virus infection [57]. Furthermore, a correlation has been noted between inflammatory mediators and oxidative stress markers in patients with severe COVID-19, particularly between IL-6 levels and the oxidative stress index [58].

Hence, the impact of compounds **1** and **4** on ROS production was also examined in the A549 cytokine model. Stimulation of A549 cells with TNF-α and IFN-γ resulted in a significant increase ($p < 0.0001$) in intracellular ROS levels, as assessed by flow cytometry using DCFH-DA (Figure 6C). When compared to the control group, compound **1** at 15 μM reduced the ROS index by 49% ($p < 0.001$). Interestingly, compound **4** exhibited values nine-fold higher ($p < 0.0001$) than the basal level, indicating a notable impact on ROS production.

Some sesquiterpene lactones have been documented to elevate intracellular ROS production, with this mechanism attributed to the induction of apoptosis in tumor cells [40]. In contrast, sesquiterpene lactones from *Artemisia austroyunnanensis* were found to decrease ROS levels in a concentration-dependent manner in LPS-stimulated RAW264.7 cells [59]. Additionally, four sesquiterpene lactones isolated from *Schkuhria pinnata* exhibited moderate ROS inhibition in the same model [60]. These findings underscore the diverse effects of sesquiterpene lactones on ROS regulation, which can vary depending on the specific compound and cellular context.

Coumarins are recognized as a class of compounds capable of inhibiting ROS-producing enzymes and are associated with chelating and radical scavenging actions [61]. The antioxidant properties of umbelliferone are attributed to its radical scavenging, metal chelation, and lipid peroxidation inhibition capabilities [49]. However, it has been reported that umbelliferone can also increase intracellular ROS levels, thereby inducing apoptosis in cancer cells. For instance, in human gastric cancer (MKN-45) and human pancreatic cancer (MIA PaCa-2) cell lines, umbelliferone was found to elevate intracellular ROS levels by 14% and 41%, respectively [62]. Similarly, KB cells (human oral carcinoma) treated with umbelliferone at 50, 100, and 150 μM exhibited a moderate increase in ROS levels (40%, 41%, and 42%, respectively) compared to untreated cells [63]. Furthermore, studies involving 7,8-diacetylated arylcoumarins [64], 3-arylcoumarin derivatives [65], and 7,8-dihydroxy-4-methylcoumarin [66] have also demonstrated an increase in intracellular ROS levels in human lung adenocarcinoma cell lines. These findings illustrate the dual nature of coumarins in modulating ROS levels, which can vary depending on the specific compound and cellular context.

2.5 | Effect of Compounds on SARS-CoV-2 Replication

In order to explore the antiviral potential of compounds **1–4**, they were evaluated in Calu-3 cells infected with SARS-CoV-2. Prior to the assays, the compounds underwent testing for cell viability, demonstrating no toxicity at the concentrations tested (Figure S4). The antiviral activity was determined using plaque assay, and the results are presented in Figure 7. The virus yield recovered after treatment with the different compounds was assessed through plaque assay in Vero CCL81 cells. All compounds exhibited anti-SARS-CoV-2 activity at both concentrations, with a reduction in viral load of approximately 1.7–2.0 log observed at 7.5 μM.

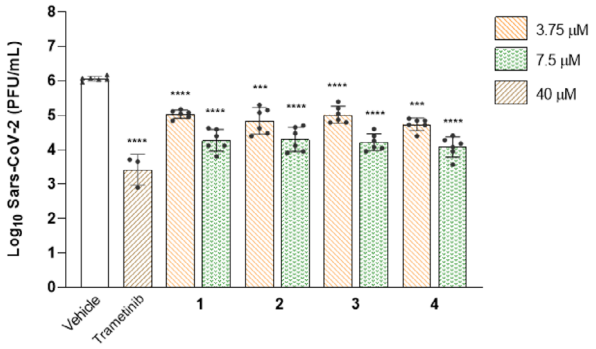

FIGURE 7 | Viral titration of supernatants from Calu-3 cells infected with Sars-CoV-2 and treated with compounds (**1–4**) isolated from *Campovassouria cruciata*. Plaque assays were performed with supernatants from Calu-3 cells (10^5 cells/well) infected with Sars-CoV-2 (MOI 0.1) during 48 h and titrated on Vero CCL81 cells overlaid with 0.8% carboxymethylcellulose. Calu-3 cells were pre-treated 1 h prior to infection with SARS-CoV-2. Treatments of infected monolayers were kept until 48 hpi, when the supernatant was collected and assayed for infectivity using plaque assay. The data obtained were expressed in plaque-forming units per milliliter (PFU/mL) and % cell viability, compared with vehicle (DMSO + ethanol) (mock: cell + virus) (positive control: trametinib 40 μM) ($n = 6$; $n = 3$ for trametinib) (***$p < 0.001$ and ****$p < 0.0001$—ANOVA with Tukey post-test).

Umbelliferone has been previously reported to inhibit TMPRSS2 (transmembrane serine protease 2) and ACE2 (angiotensin-converting enzyme 2), which are both essential for the entry of SARS-CoV-2 into cells. This inhibition was demonstrated through FRET-based enzymatic assays and molecular docking analysis [67]. To the best of our knowledge, this study represents the initial report demonstrating the inhibition of SARS-CoV-2 by umbelliferone in Calu-3-infected cells. This finding underscores the promising potential of umbelliferone as an antiviral agent and warrants further investigation into its therapeutic application against SARS-CoV-2.

This study also marks the first report of the anti-SARS-CoV-2 activity of **leptocarpin** and **arturin**. Previous in silico investigations have pointed out the potential antiviral effects of sesquiterpene lactones against SARS-CoV-2 proteins. Hence, reynosin and 4-fluoro-santamarin have exhibited potential activity against the Mpro protease, RNA replicase, and Spike protein in molecular docking analyses [27]. Moreover, the potent antimalarial compound artemisinin and its derivatives have demonstrated the ability to bind to the active site of Mpro, particularly at residue Cys145, thereby inhibiting the proteolytic process crucial for virus replication [28]. Ávila-Gálvez et al. [68] have discovered a potential inhibitory activity of chicory extract against both the Mpro and a papain-like protease (PLpro) of SARS-CoV-2.

Subsequently, the four most abundant sesquiterpene lactones identified in this extract were shown to be responsible for the inhibition of these proteases, effectively binding to their active sites. Therefore, sesquiterpene lactones exhibit promising anti-SARS-CoV-2 activity, as demonstrated by literature data and also by our results in Calu-3 infected cells, which deserve further investigation.

3 | Conclusions

The phytochemical investigation of *C. cruciata* yielded four compounds described here for the first time in the species, including the novel sequiterpene lactone **3-*epi*-leptocarpin**, alongside **leptocarpin** and **arturin**. All resonance signals of these compounds were unequivocally assigned through extensive mono- and two-dimensional ^{1}H and ^{13}C NMR data analysis. **Umbeliferone** and **3-*epi*-leptocarpin** significantly inhibited IL-6 and IL-8 release and ROS production in A549 cells previously stimulated with IFN-γ and TNF-α. Besides, all four isolated compounds inhibited SARS-CoV-2 replication in Calu-3 cells. Collectively, our findings highlight *C. cruciata* as a promising source of bioactive sesquiterpene lactones and coumarins, warranting further investigation for their potential development as novel therapeutic agents against inflammatory and viral diseases.

4 | Experimental Section

4.1 | General Experimental Procedures

Optical rotations were recorded on a Bellingham & Stanley ADP 220 Polarimeter. IR spectra were measured on Shimadzu IRSpirit-T spectrophotometer. NMR spectra were recorded on Bruker Avance NEO 600 MHz and Bruker Avance III HD 400 MHz. Spectra were recorded in acetone-d6 (for 1) or CDCl3 (for 2–4) and processed by Bruker TopSpin 4.1 software. Tetramethylsilane (TMS) was used as an internal reference; chemical shifts are reported as δ values (ppm) and J in Hz. The chromatograms and mass spectra were obtained on a UPLC-MS/MS ACQUITY Ultra Performance LCTM system (Waters), with a diode array detector (PDA 2996), a mass spectrometer ACQUITY TQ (Waters), electron-Z spray ionization (ESI), and software MassLynx (versão 4.1, Waters). A Waters UPLC column (Acquity UPLC BEH HILIC; 150 × 2.1 mm^2, 1.7 μm) equipped with a pre-column (UPLC BEH HILIC; 5 × 2.1 mm^2, 1.7 μm, Waters) was used, with a flow rate of 0.300 mL/min. The elution was performed using a gradient of CH_3CN and deionized H_2O containing 0.1% formic acid (0–10 min, 5%–95% CH_3CN; 10–15 min, isocratic condition at 95% CH_3CN; 15–16 min, 95%–5% CH_3CN; 16–18 min, isocratic condition at 5% CH_3CN). The UV detection was performed in 205–500 nm range. The ESI/MS detection was accomplished with positive and negative mode ionization (TQ) with an m/z range of 20–2000 Da. Collision energy, 15–70 eV; capillary 3.5 kV; cone voltage 3 V; gas temperature and desolvation 350°C and 550 L/h. The preparative high-performance liquid chromatography (HPLC) was executed on an RP-HPLC Waters system, consisting of a binary solvent pump (Waters 1525 Binary HPLC Pump) connected to a photodiode array detector (Waters 2489 UV-Visible Detector) and a fraction collector (Waters 2707 Autosampler). For purification, a Prep-C18 (21.2 × 250 mm^2, 10 μm, Agilent) column was used. Column chromatographic purification of compounds was performed on silica gel (40−63 μm, Aldrich Chemistry). TLC was carried out on silica plates (TLC silica 60 F254, Merck), and zones were detected by spraying with sulfuric anisaldehyde, followed by heating. The optical density for the assays was read with a Varioskan Lux (Thermo Scientific) using (SkanIt Software). The enzyme-linked immunosorbent assay (ELISA) kits for the cytokines were acquired from R&D Systems (DY210 human TNF duo set, DY206 human IL-6 duo set, DY208 human IL-8 duo set, R&D Systems, Minneapolis, MN, USA). Intracellular analysis of ROS was performed by LSRFortessa flow cytometer (BD Biosciences Pharmingen, California, USA) FCAP Array Software version 1.0.1.

4.2 | Plant Material

The plant material was collected in the states of Minas Gerais, Espírito Santo, and Rio de Janeiro, Brazil, by Geraldo Wilson Fernandes (collection date: 06/2018) and identified by the taxonomist Gustavo Heiden. The voucher specimens are deposited in the Herbarium of Embrapa Clima Temperado, RS, Brazil (*B. brevifolia* DC.—ECT 6259/*B. calvescens* DC.—ECT 5549/*B. imbricata* Malag. ECT 5912/*C. cruciata* (Vell.) R.M.King & H Rob—ECT 5985/*B. oblongifolia* (Ruiz & Pav.) Pers—ECT 5930/*B. stylosa* Gardner—ECT 5950) (SisGen A5BF5D0).

4.3 | Extraction and Isolation

After drying at 40°C and pulverization, the leaves of each species were percolated with EtOH. The solvent was removed in a rotary evaporator, under reduced pressure, at a maximum temperature of 45°C, and subsequently, the extracts were lyophilized. Part of the *C. cruciata* extract (2 g) was solubilized in 100 mL of methanol/water solution (3:7) and partitioned with HEX, DCM, and EtOAc (3 × 50 mL^2 each). The solvents were evaporated, and three fractions were obtained: HEX fraction (480 mg), DCM fraction (280 mg), and EtOAc fraction (438 mg). Subsequently, the same procedure was performed with 16 g of extract to obtain a greater amount of the DCM fraction (3 g).

Part of DCM fraction (2.0 g) was fractionated by column chromatography on silica gel (38 × 4.2 cm^2 i.d.) with a gradient of HEX/DCM/EtOAc [40:60:0–0:100:0–0:50:50] as a mobile phase. Fractions of 10 mL were collected and combined according to their TLC profiles, resulting in 28 grouped fractions. Fractions Fr. 166–191, Fr. 220–247, and Fr. 255–279 were used for further purification.

Fr. 166–191 (139.7 mg) was purified with DCM. The suspension was centrifuged for 10 min at 7.000 × g, and the supernatant was removed. The procedure was repeated five times. A white solid precipitate was obtained (62.4 mg), corresponding to compound **4**.

Fr. 200–247 (336.5 mg) was purified on a silica gel column (70 cm × 1.5 cm i.d.) with a HEX/EtOAc gradient resulting in seven grouped fractions, combined on the basis of TLC patterns. The C2-D fraction was submitted to preparative RP-HPLC (Waters 1525 Binary HPLC Pump/Waters 2489 UV-Visible

Detector/Waters 2707 Autosampler), and the elution was performed with a gradient of CH_3CN and water, from 10% to 95% CH_3CN in 41 min, followed by 4 min of isocratic elution of 95% CH_3CN at a flow rate of 14mL/min. Detection was set at 225 and 254 nm. The solvent of the collected fractions was removed by evaporation under reduced pressure followed by lyophilization and resulted in compound **2** (Rt = 27.5 min; 94.6 mg) and compound **3** (Rt = 33.2 min; 17.3 mg).

Fr. 255–279 (232.7 mg) was further separated by chromatography on a silica gel column (70 cm × 1.5 cm i.d.), and the elution was performed with a gradient of HEX and EtOAc. The fractions were also combined on the basis of TLC patterns and resulted in seven grouped fractions. The C3-D fraction afforded compound **1** (15.8 mg).

3-*epi*-leptocarpin (**1**): white microcrystalline powder. λ_{max} (log ε, acetonitrile) 228 (2.0) nm. ^{1}H NMR and ^{13}C NMR, Table 1. ESIMS m/z 363 $[M + H]^+$. $[\alpha]_D$ −49.1° ($CHCl_3$). IR 3428, 1747, 1389, 1122, 977 cm^{-1}.

Leptocarpin (**2**): white microcrystalline powder. λ_{max} (log ε, acetonitrile) 228 (2.4) nm. ^{1}H NMR and ^{13}C NMR, Table 1. ESIMS m/z 363 $[M + H]^+$. $[\alpha]_D$ −100° ($CHCl_3$). IR 3422, 2919, 2876, 1753, 1720, 1154, 1135, 974 cm^{-1}.

Arturin (**3**): white microcrystalline powder. λ_{max} (log ε, acetonitrile) 224 (2.4) nm. ^{1}H NMR and ^{13}C NMR, Table 1. ESIMS m/z 347 $[M + H]^+$. $[\alpha]_D$ −100° ($CHCl_3$). IR 3432, 2944, 1759, 1714, 1231, 1142, 1022, 993, 966 cm^{-1}.

Umbelliferone (**4**): white amorphous powder. ^{1}H NMR (400 MHz, acetone-d_6) δ_H 6.17 (d, 9.4 Hz, H-3), 7.86 (d, 9.4 Hz, H-4), 7.51 (d, 8.2 Hz, H-5), 6.84 (d, 8.2 Hz, H-6), 6.75 (s, H-8). 13C NMR (100 MHz, acetone-d6) δC 162.0 (C-2), 112.7 (C-3), 144.6 (C-4), 130.4 (C-5), 113.7 (C-6), 161.0 (C-7), 103.2 (C-8), 112.8 (C-9), 156.9 (C-10). ESIMS m/z 163 $[M + H]^+$, 161 $[M–H]^-$. IR 3122, 1704, 1678, 1601, 833 cm^{-1}.

4.4 | Cells and Culture Conditions

L929 (murine fibroblasts, ATCC CCL-1), A549 (human lung carcinoma fibroblast—CCL-185), and VERO E6 (African green monkey kidney epithelial cells, ATCC, CRL1586) cells were maintained and cultured in RPMI (Thermo Fisher Scientific, MA, USA) supplemented with 10% fetal bovine serum (FBS, Gibco, Thermo Fisher, Monza, Italy) at 37°C in a 5% CO_2 atmosphere. Calu-3 (human lung adenocarcinoma, ATCC HTB-55) cells were cultured in high-glucose Dulbecco's Modified Eagle Medium (DMEM, Thermo Fisher Scientific) supplemented with 1% L-glutamine, 10% FBS, 1% non-essential amino acid (NEAA), and 1% sodium pyruvate solution under a controlled atmosphere (37°C and 5% CO_2).

4.5 | Coronavirus

Andrade et al. (2021) [69] describe the MHV-3 strain obtained from Clarice Weis Arns and Ricardo Durães-Carvalho at the Universidade Estadual de Campinas (UNICAMP, Brazil). The strain was provided, and its genome was sequenced (GenBank accession no. MW620427.1). The virus was propagated in L929 cells. SARS-CoV-2 was cultured in Vero ATCC CCL81 using an isolate obtained from a nasopharyngeal swab of a confirmed COVID-19 case in Rio de Janeiro, Brazil (GenBank accession no. MT710714), following the guidelines established by the WHO.

4.6 | Cell Viability Assay

To determine the viability of extracts, fractions, and compounds, the mitochondrial reduction assay MTT was performed. The cells were cultivated in a 96-well plate (1 × 104 cells/well) and incubated overnight at 37°C in a 5% CO_2 atmosphere. Subsequently, 100 µL of each sample solution prepared at different concentrations (10–90 µg/mL for extract and fractions; 1–15 µM for isolated compounds) in RPMI or DMEM 2% FBS were added to the wells. After 24 h of incubation, the medium was removed, and 100 µL of MTT solution (2 mg/mL) was added, followed by an additional 4-h incubation. The absorbance was measured at 570 nm, and the data were expressed as a percentage of control cells (cultured in the absence of the sample), which were considered 100% viable. The assays were carried out in triplicate.

4.7 | Antiviral of the Samples and Plaque Assay

For the evaluation of the antiviral activity of the extract, fractions, and isolated compounds, murine (L929) and human (Calu-3) cells were seeded into 24-well plates. The cells were pre-treated with the natural compounds for 1 h and then infected with MHV-3 (MOI 0.01) and SARS-CoV-2 (MOI 0.1).

For viral titration, 100 µL of serially diluted virus suspension (diluted 1:9 in RPMI) was inoculated onto confluent monolayers of L929 cells (for MHV-3) or Vero CCL81 cells (for SARS-CoV-2) grown in 24-well plates. Inoculated plates were incubated at 37°C for 1 h in a CO_2 incubator (with agitation every 15 min). After incubation, the inoculated samples were removed, and an overlay medium (consisting of RPMI containing 0.8% carboxymethylcellulose and 2% FBS) was added to each well. The plates were then kept at 37°C with 5% CO_2 for 2 days (for MHV-3) or 3 days (for SARS-CoV-2). Following incubation, the cells were fixed with 10% neutral buffered formalin for 1 h and subsequently stained with 0.1% crystal violet. The virus titers were determined as plaque-forming units (PFUs).

4.8 | Cytokine Release in A549 Cells

The compounds were also evaluated for their potential anti-inflammatory activity in lung cells. A549 cells were pre-treated with or without extract, fractions, or isolated compounds for 3 h and then stimulated with 10 ng/mL of TNF-α and 10 ng/mL of IFN-γ. After 24 h, the cell supernatants were collected for cytokine immunoassay. Simultaneously, the cells were washed with PBS, cells/wells were trypsinized, and they were labeled with an intracellular probe to measure ROS levels.

4.9 | Cytokine Measurement

Supernatants were centrifuged at 10 000 × *g* for 10 min and quantified IL-6, IL-8, and TNF-α levels using ELISA kits (DuoSet, R&D Systems) in accordance with the manufacturer's instructions. The concentrations of cytokines were expressed in pg/mL of supernatant.

4.10 | Production of Intracellular ROS

Intracellular levels of ROS production were evaluated using the oxidation-sensitive dye DCFH-DA. A549 cells were cultured in 24-well plates at a density of 105 cells/well and incubated for 24 h at 37°C in a 5% CO_2 atmosphere. The protocol outlined previously by Aranda et al. (2013) [70] was followed for conducting these experiments. To quantify the generation of intracellular ROS, following the collection of supernatants, cells were washed with PBS and subsequently stained with DCFH-DA (10 μM) for 20 min at room temperature, shielded from light. DCF fluorescence (with an excitation wavelength of 485 nm and an emission wavelength of 535 nm) in PBS was measured using a Fortessa flow cytometer (BD Biosciences Pharmingen, California, USA), and the acquired data were analyzed using FlowJo software.

Supporting Information

The viability assays of extracts, fractions, and isolated compounds in L929, A549, and Calu-3 cells are available as supporting information, along with UV and mass spectra (ESI+ and ESI-) of peaks 1, 2, 3 and 4, and IR, ^{1}H NMR, ^{13}C NMR, ^{1}H–^{1}H COSY, HSQC, HMBC, and NOESY spectra of compounds 1–4.

Author Contributions

Maria Beatriz de O. Rabelo: investigation, methodology, visualization, writing – original draft. **Kátia M. Freitas**: investigation, methodology, writing – review and editing. **Leonardo C. de Oliveira**: investigation, methodology. **Alessandra C. M. Frade**: methodology. **José D. de S. Filho**: methodology. **Gustavo Heiden**: resources. **Geraldo W. Fernandes**: resources. **Izabella Thaís da Silva**: resources. **Mauro Martins Teixeira**: resources. **Fernão C. Braga**: funding acquisition, supervision, writing – review and editing. **Rodrigo M. Pádua**: funding acquisition, supervision, writing – review and editing.

Acknowledgments

CAPES (Brazil) is acknowledged for a postdoctoral fellowship (K.M.F.) and the Conselho Nacional de Pesquisa (CNPq/Brazil) for a research fellowship (F.C.B.). We acknowledge the Fundação de Amparo à Pesquisa do Estado de Minas Gerais (FAPEMIG/Brazil) for the financial support to the NMR spectroscopy facility (LAREMAR/UFMG; grant number APQ-01848-22) and for a PhD fellowship (M.B.O.R.).

Conflicts of Interest

The authors declare no conflicts of interest.

Data Availability Statement

The authors have nothing to report.

References

1. T. G. Ksiazek, D. Erdman, C. S. Goldsmith, S. R. Zaki, and T. Peret, "A Novel Coronavirus Associated With Severe Acute Respiratory Syndrome," *New England Journal of Medicine* 348 (2003): 1953–1966.

2. C. Drosten, S. Günther, W. Preiser, et al., "Identification of a Novel Coronavirus in Patients With Severe Acute Respiratory Syndrome," *New England Journal of Medicine* 348 (2003): 1967–1976.

3. A. M. Zaki, S. Van Boheemen, T. M. Bestebroer, A. D. M. E. Osterhaus, and R. A. M. Fouchier, "Isolation of a Novel Coronavirus From a Man With Pneumonia in Saudi Arabia," *New England Journal of Medicine* 367 (2012): 1814–1820.

4. B. L. Haagmans, S. H. S. Al Dhahiry, C. B. E. M. Reusken, and V. S. Raj, "Middle East Respiratory Syndrome Coronavirus in Dromedary Camels: An Outbreak Investigation," *Lancet Infect* 14 (2014): 140–145.

5. H. Li, Y. Zhou, M. Zhang, H. Wang, and Q. Zhao, "Updated Approaches against SARS-CoV-2," *Antimicrobial Agents and Chemotherapy* 64 (2020): 1–7.

6. N. Zhu, D. Zhang, W. Wang, et al., "A Novel Coronavirus From Patients With Pneumonia in China, 2019," *New England Journal of Medicine* 382 (2020): 727–733.

7. World Health Organization, *COVID-19 Weekly Epidemiological Update* (WHO, 2024).

8. S. Ludwig and A. Zarbock, "Coronaviruses and SARS-CoV-2: A Brief Overview," *Anesthesia and Analgesia* 131 (2020): 93–96.

9. T. U. Singh, S. Parida, M. C. Lingaraju, M. Kesavan, D. Kumar, and R. K. Singh, "Drug Repurposing Approach to Fight COVID-19," *Pharmacological Reports* 72 (2020): 1479–1508.

10. A. Tuekprakhon, R. Nutalai, A. Dijokaite-Guraliuc, et al., "Antibody Escape of SARS-CoV-2 Omicron BA.4 and BA.5 From Vaccine and BA.1 Serum," *Cell* 185 (2022): 2422–2433.e13.

11. A. M. Shaqra, S. N. Zvornicanin, Q. Y. J. Huang, et al., "Defining the Substrate Envelope of SARS-CoV-2 Main Protease to Predict and Avoid Drug Resistance," *Nature Communications* 13 (2022): 1–11.

12. D. J. Newman and G. M. Cr, "Natural Products as Sources of New Drugs Over the Nearly Four Decades From 01/1981 to 09/2019," *Journal of Natural Products* 83 (2020): 770–803.

13. S. Verma, D. Twilley, T. Esmear, et al., "Anti-SARS-CoV Natural Products With the Potential to Inhibit SARS-CoV-2 (COVID-19)," *Frontiers in Pharmacology* 11 (2020): 1–20.

14. Z. Wang, N. Wang, L. Yang, and X. Q. Song, "Bioactive Natural Products in COVID-19 Therapy," *Frontiers in Pharmacology* 13 (2022): 1–14.

15. J. I. Achika, D. E. Arthur, I. Gerald, and A. Adedayo, "A Review on the Phytoconstituents and Related Medicinal Properties of Plants in the Asteraceae Family," *IOSR Journal of Applied Chemistry* 7 (2014): 01–08.

16. M. Valli, H. M. Russo, and V. S. da Bolzan, "The Potential Contribution of the Natural Products From Brazilian Biodiversity to Bioeconomy," *Anais Da Academia Brasileira De Ciencias* 90 (2018): 763–778.

17. L. G. Verdi, I. Maria, C. Brighente, et al., "Gênero Baccharis (Asteraceae): Aspectos químicos, econômicos e biológicos," *Quimica Nova* 28 (2005): 85–94.

18. E. K. O. Hattori, "Filogenia Molecular Da Subtribo Disynaphiinae (Eupatorieae: Asteraceae)," *Tratamento Taxonômico e Sinopse De Symphyopappus* (Universidade Federal de Minas Gerais, 2013).

19. R. Campos, J. Bressan, V. Cristina, et al., "Baccharis (Asteraceae): Chemical Constituents and Biological Activities," *Chemistry and Biodiversity* 13 (2016): 1–17.

20. A. N. De Gutierrez, A. Bardón, C. A. N. Catalán, T. B. Gedris, and W. Herz, "Sesquiterpene Lactones and Other Constituents of *Disynaphia multicrenulata* From Argentina," *Biochemical Systematics and Ecology* 29 (2001): 633–647.

21. F. B. Da Costa, L. Terfloth, and J. Gasteige, "Sesquiterpene Lactone-Based Classification of Three Asteraceae Tribes: A Study Based on Self-Organizing Neural Networks Applied to Chemosystematics," *Phytochemistry* 66 (2005): 345–353.

22. R. Kaul, P. Paul, S. Kumar, D. Büsselberg, V. D. Dwivedi, and A. Chaari, "Promising Antiviral Activities of Natural Flavonoids against Sars-CoV-2 Targets: Systematic Review," *International Journal of Molecular Sciences* 22 (2021): 1–50.

23. S. Jo, S. Kim, D. H. Shin, and M. S. Kim, "Inhibition of SARS-CoV 3CL Protease by Flavonoids," *Journal of Enzyme Inhibition and Medicinal Chemistry* 35 (2020): 145–151.

24. S. Singh, M. F. Sk, A. Sonawane, P. Kar, and S. Sadhukhan, "Plant-Derived Natural Polyphenols as Potential Antiviral Drugs against SARS-CoV-2 via RNA-dependent RNA Polymerase (RdRp) Inhibition: An in-Silico Analysis," *Journal of Biomolecular Structure & Dynamics* 39 (2021): 6249–6264.

25. C. M. Leal, S. G. Leitão, R. Sausset, et al., "Flavonoids From *Siparuna cristata* as Potential Inhibitors of SARS-CoV-2 Replication," *Revista Brasileira De Farmacognosia* 31 (2021): 658–666.

26. F. Bohlmann, C. Zdero, R. M. King, and H. Robinson, "8β-Tigloylguaiagrazielolide From *Campovassouria bupleurifolia*," *Phytochemistry* 22 (1983): 2860–2862.

27. F. J. R. Mejías, A. G. Durán, N. Chinchilla, et al., "In Silico Evaluation of Sesquiterpenes and Benzoxazinoids Phytotoxins Against Mpro, RNA Replicase and Spike Protein of SARS-CoV-2 by Molecular Dynamics. Inspired by Nature," *Toxins (Basel)* 14 (2022): 1–18.

28. R. Badraoui, M. Saoudi, W. S. Hamadou, et al., "Antiviral Effects of Artemisinin and Its Derivatives Against SARS-CoV-2 Main Protease: Computational Evidences and Interactions With ACE2 Allelic Variants," *Pharmaceuticals* 2022 (2022): 129.

29. A. E. Abe, C. E. De Oliveira, T. M. Dalboni, et al., "Anti-Inflammatory Sesquiterpene Lactones From *Tithonia diversifolia* Trigger Different Effects on Human Neutrophils," *Revista Brasileira De Farmacognosia* 25 (2015): 111–116.

30. F. Wang, H. Zhong, S. Fang, et al., "Potential Anti-Inflammatory Sesquiterpene Lactones from *Eupatorium lindleyanum*," *Planta Medica* 84 (2018): 123–128.

31. R. W. Körner, M. Majjouti, M. A. Alejandre Alcazar, and E. Mahabir, "Of Mice and Men: The Coronavirus MHV and Mouse Models as a Translational Approach to Understand SARS-CoV-2," *Viruses* 12 (2020): 880, https://doi.org/10.3390/v12080880.

32. G. Ryu and H. W. Shin, "SARS-CoV-2 Infection of Airway Epithelial Cells," *Immune Network* 21 (2021): 1–16.

33. S. Ramirez, C. Fernandez-Antunez, A. Galli, et al., "Overcoming Culture Restriction for SARS-CoV-2 in Human Cells Facilitates the Screening of Compounds Inhibiting Viral Replication," *Antimicrobial Agents and Chemotherapy* 65 (2021): 1–20.

34. B. Drasler, B. B. Karakocak, E. B. Tankus, et al., "An Inflamed Human Alveolar Model for Testing the Efficiency of Anti-Inflammatory Drugs In Vitro," *Frontiers in Bioengineering and Biotechnology* 8 (2020): 1–21.

35. J. Gong, H. Dong, Q. S. Xia, et al., "Correlation Analysis between Disease Severity and Inflammation-Related Parameters in Patients with COVID-19: A Retrospective Study," *BMC Infectious Diseases* [Electronic Resource] 20 (2020): 1–7.

36. L. Sapra, A. Bhardwaj, Z. Azam, et al., "Phytotherapy for Treatment of Cytokine Storm in COVID-19," *Frontiers in Bioscience—Landmark* 26 (2021): 51–75.

37. M. Maas, A. M. Deters, and A. Hensel, "Anti-Inflammatory Activity of *Eupatorium perfoliatum* L. Extracts, Eupafolin, and Dimeric Guaianolide via iNOS Inhibitory Activity and Modulation of Inflammation-Related Cytokines and Chemokines," *Journal of Ethnopharmacology* 137 (2011): 371–381.

38. C. Chu, H. Ren, N. Xu, L. Xia, D. Chen, and J. Zhang, "*Eupatorium lindleyanum* DC. Sesquiterpenes Fraction Attenuates Lipopolysaccharide-Induced Acute Lung Injury in Mice," *Journal of Ethnopharmacology* 185 (2016): 263–271.

39. R. Martinez, I. S. Ayamante, J. Núñez-Alarcón, and A. Romo De Vivar, "Leptocarpin and 17,18-Dihydroleptocarpin, Two New Heliangolides From *Leptocarpha rivularis*," *Phytochemistry* 18 (1979): 1527–1528.

40. D. Chaturvedi, *Opportunity, Challenge and Scope of Natural Products in Medicinal Chemistry* (Research Signpost, 2011).

41. N. H. Fischer, "Sesquiterpenes Lactones: Biogenesis and Biomimetic Transformations," in *Biochemistry of the Mevalonic Acid Pathway to Terpenoids*, ed. G. H. N. Towers, H. A. Stafford (Springer, 1990), 1–352.

42. Y. C. Shen, K. L. Lo, Y. H. Kuo, and A. T. Khalil, "Cytotoxic Sesquiterpene Lactones From Eupatoriumkiirunense, a Coastal Plant of Taiwan," *Journal of Natural Products* 68 (2005): 745–750.

43. M. Holub and Z. Samek, "Isolation and Structure of 3-Epinobilin, 1,10-Epoxynobilin and 3-Dehydronobilin—Other Sesquiterpenic Lactones From the Flowers of *Anthemis nobilis* L. Revision of the Structure of Nobilin and Eucannabinolide," *Collection of Czechoslovak Chemical Communications* 42 (1977): 1053–1064.

44. A. G. Ober, F. R. Fronczek, and N. H. Fischer, "Sesquiterpene Lactones of *Calea divaricata* and the Molecular Structure of Leptocarpin Acetate," *Journal of Natural Products* 48 (1985): 302–306.

45. R. Martinez, V. Kesternich, E. Gutierrez, H. Dölz, and H. Mansilla, "Conformational Analysis and Biological Activity of Leptocarpin and Leptocarpin Acetate," *Planta Medica* 61 (1995): 188–189.

46. H. Maritza, M. Sicva, and F. Botiliviannt, "Sesquiterpenes lactones of Podanthus mitiqui," *Phytochemistry* 19 (1980): 2765–2766.

47. C. L. Cespedes, M. Hoeneisen, M. Bittner, J. Becerra, and M. Silva, "Comparative Study of Ovatifolin Antioxidant and Growth Inhibition Activities," *Journal of Agricultural and Food Chemistry* 49 (2001): 4243–4251.

48. H. Wagner and S. Bladt, *Plant Drug Analysis: A Thin Layer Chromatography Atlas* (Springer, 1996).

49. O. Mazimb, "Umbelliferone: Sources, Chemistry and Bioactivities Review," *Bulletin of Faculty of Pharmacy, Cairo University* 55 (2017): 223–232.

50. T. J. T. de Souza, S. A. L. Bordignon, M. A. Apel, and A. T. Henriques, "Volatile Constituents of Eupatorieae (Asteraceae). Compositional Multivariate Analysis of Volatile Oils From Southern Brazilian Species in the Subtribe Disynaphiinae," *Phytochemistry* 186 (2021): 1–23.

51. L. Li, J. Li, M. Gao, et al., "Interleukin-8 as a Biomarker for Disease Prognosis of Coronavirus Disease-2019 Patients," *Frontiers in Immunology* 11 (2021): 1–10.

52. E. H. M. Hassanein, A. M. Sayed, O. E. Hussein, and A. M. Mahmoud, "Coumarins as Modulators of the Keap1/Nrf2/ARE Signaling Pathway," *Oxidative Medicine and Cellular Longevity* 2020 (2020): 1–25.

53. D. Wang, X. Wang, W. Tong, Y. Cui, X. Li, and H. Sun, "Umbelliferone Alleviates Lipopolysaccharide-Induced Inflammatory Responses in Acute Lung Injury by Down-Regulating TLR4/MyD88/NF-κB Signaling," *Inflammation* 42 (2019): 440–448.

54. J. ye Lim, J. H. Lee, D. H. Lee, J. H. Lee, and D. K. Kim, "Umbelliferone Reduces the Expression of Inflammatory Chemokines in HaCaT Cells and DNCB/DFE-Induced Atopic Dermatitis Symptoms in Mice," *International Immunopharmacology* 75 (2019): 1–9.

55. A. Paço, T. Brás, J. O. Santos, P. Sampaio, A. C. Gomes, and M. F. Duarte, "Anti-Inflammatory and Immunoregulatory Action of Sesquiterpene Lactones," *Molecules (Basel, Switzerland)* 27 (2022): 1–22.

56. Y. K. Lee, H. Lee, Y. N. Kim, J. Kang, E. J. Jeong, and J. R. Rho, "Sesquiterpene Lactones with Anti-Inflammatory Activity from the Halophyte *Sonchus Brachyotus* DC," *Molecules* 28 (2023): 1–11.

57. I. G. Fernandes, C. A. De Brito, V. M. S. Dos Reis, M. N. Sato, and N. Z. Pereira, "SARS-CoV-2 and Other Respiratory Viruses: What Does Oxidative Stress Have to Do With It?," *Oxidative Medicine and Cellular Longevity* 2020 (2020): 1–13.

58. M. Petrushevska, D. Zendelovska, E. Atanasovska, A. Eftimov, and K. Spasovska, "Presentation of Cytokine Profile in Relation to Oxidative Stress Parameters in Patients with Severe COVID-19: An Observational Pilot Study," *F1000Research* 10 (2021): 1–14.

59. L. Liu, D. Liu, C. Xiang, W. Dai, B. Li, and M. Zhan, "Sesquiterpene Lactones From *Artemisia austroyunnanensis* Suppresses ROS Production and Reduces Cytokines, iNOS and COX-2 Levels via NF-KB Pathway In Vitro," *Natural Product Research* 34 (2020): 1563–1566.

60. R. G. Kudumela, O. Mazimba, and P. Masoko, "Characterisation of Sesquiterpene Lactones from *Schkuhria pinnata* and Their Antibacterial and Anti-Inflammatory Activities,"*South African Journal of Botany* 126 (2019): 340–344.

61. L. Todorov, L. Saso, and I. Kostov, "Antioxidant Activity of Coumarins and Their Metal Complexes," *Pharmaceuticals* 16 (2023): 1–26.

62. Ö. S. Aslantürk and T. A. Çelik, "Anticancer Effect of Umbelliferone on MKN-45 and MIA PaCa-2 Cell Lines," *Toxicology In Vitro* 93 (2023): 1–10.

63. A. Vijayalakshmi and G. Sindhu, "Umbelliferone Arrest Cell Cycle at G0/G1 Phase and Induces Apoptosis in Human Oral Carcinoma (KB) Cells Possibly via Oxidative DNA Damage," *Biomedicine and Pharmacotherapy* 92 (2017): 661–671.

64. M. A. Musa and Q. Kolawole, "7,8-Diacetoxy-3-(4-Methylsulfonylphenyl)-4-Phenylcoumarin Induces ROS-Dependent Cell Death in the A549 Human Lung Cancer Cell Line," *Anticancer Research* 43 (2023): 1001–1007.

65. M. A. Musa, M. Y. Joseph, L. M. Latinwo, V. Badisa, and J. S. Cooperwood, "*In Vitro* Evaluation of 3-Arylcoumarin Derivatives in A549 Cell Line," *Anticancer Research* 35 (2015): 653–659.

66. A. Goel, A. K. Prasad, V. S. Parmar, B. Ghosh, and N. Sain, "7,8-Dihydroxy-4-Methylcoumarin Induces Apoptosis of Human Lung Adenocarcinoma Cells by ROS-Independent Mitochondrial Pathway Through Partial Inhibition of ERK/MAPK Signaling," *FEBS Letters* 581 (2007): 2447–2454.

67. F.-J. Cheng, C.-Y. Ho, T.-S. Li, et al., "Umbelliferone and Eriodictyol Suppress the Cellular Entry of SARS-CoV-2," *Cell & Bioscience* 13 (2023): 1–19.

68. M. Á. Ávila-Gálvez, C. Rafael-Pita, N. Fernández, et al., "Targeting Proteases Involved in the Viral Replication of SARS-CoV-2 by Sesquiterpene Lactones From Chicory (*Cichorium intybus* L.)," *Food Function* 13 (2022): 8977–8988.

69. A. C. dos S. P. Andrade, G. H. Campolina-Silva, C. M. Queiroz-Junior, et al., "A Biosafety Level 2 Mouse Model for Studying Betacoronavirus-Induced Acute Lung Damage and Systemic Manifestations," *Journal of Virology* 95 (2021): 1–18.

70. A. Aranda, L. Sequedo, L. Tolosa, et al., "Dichloro-Dihydro-Fluorescein Diacetate (DCFH-DA) Assay: A Quantitative Method for Oxidative Stress Assessment of Nanoparticle-Treated Cells," *Toxicology in Vitro* 27 (2013): 954–963.

Supporting Information

Additional supporting information can be found online in the Supporting Information section.